

Short-range and tensor correlations in the $^{16}\text{O}(e,e'pn)$ reaction

C. Giusti¹, H. Mütter², F. D. Pacati¹ and M. Stauf²

¹*Dipartimento di Fisica Nucleare e Teorica dell'Università, Pavia
and Istituto Nazionale di Fisica Nucleare, Sezione di Pavia, Italy*

²*Institut für Theoretische Physik, Universität Tübingen,
Auf der Morgenstelle 14, D-72076 Tübingen, Germany*

(August 31, 2018)

The cross sections for electron induced two-nucleon knockout reactions are evaluated for the example of the $^{16}\text{O}(e,e'pn)^{14}\text{N}$ reaction leading to discrete states in the residual nucleus ^{14}N . These calculations account for the effects of nucleon-nucleon correlations and include the contributions of two-body meson exchange currents as the pion seagull, pion in flight and the isobar current contribution. The effects of short-range as well as tensor correlations are calculated within the framework of the coupled cluster method employing the Argonne V14 potential as a model for a realistic nucleon-nucleon interaction. The relative importance of correlation effects as compared to the contribution of the meson exchange currents depends on the final state of the residual nucleus. The cross section leading to specific states, like e.g. the ground state of ^{14}N , is rather sensitive to the details of the correlated wave function.

PACS numbers: 24.10.Cn, 25.30.Fj, 27.20.+n

I. INTRODUCTION

The nuclear shell-model, describing a nucleus as a system of nucleons moving in a mean field, describes many basic features of nuclear structure. Nevertheless, it is well known, that the strong components of a realistic model for the nucleon-nucleon (NN) interaction induce correlations into the nuclear wave function, which are beyond this mean field description. In particular one has to consider the two-nucleon short-range correlations, induced by the repulsive components of the NN interaction, and the tensor correlations which are mainly due to the strong tensor components of the pion exchange contribution to the NN interaction. A detailed investigation of these correlations should provide insight into the structure of the interaction of two nucleons in a nuclear medium. Therefore it has always been a great challenge of nuclear physics to develop experiments and theoretical models, which explore these correlations.

Photoinduced two-nucleon knockout experiments like (γ, NN) or $(e, e'NN)$ reactions seem to be a powerful tool for such investigations since the probability that a real or virtual photon is absorbed by a pair of nucleons should be a direct measure for the correlations between these nucleons. Such triple coincidence experiments have been made possible by the progress in accelerator and detector technology and first measurements of the exclusive $^{16}\text{O}(e, e'pp)^{14}\text{C}$ reaction have been performed at NIKHEF in Amsterdam [1,2] and MAMI in Mainz [3]. First investigations on these data [1–4] indicate that resolution of discrete final states provides an interesting tool to disentangle and thus separately investigate contributions of one-body currents, due to short-range correlations, and two-body isobar currents. In particular, clear signatures for short-range correlations have been obtained for the transition to the ground state of ^{14}C . This result gives rise to the hope that a similar separation between two-body currents and correlations is possible also in the $(e, e'pn)$ reaction. This would be of particular interest as tensor correlations will predominantly be present in the wave function of a pn pair. Thus $(e, e'pn)$ experiments would complete the information on NN correlations. It is obvious that such experiments are more difficult as they require a triple coincidence measurement with a detection of a neutron. A proposal for the experimental study of the exclusive $^{16}\text{O}(e, e'pn)^{14}\text{N}$ reaction has been recently approved in Mainz [5]. This first experiment will demonstrate the feasibility of triple coincidence experiments including neutrons with high resolution and will serve as exploratory study for the investigations of np correlations.

Also the theoretical analysis of the pn data is a bit more involved than the analysis of the pp data since the contribution of the correlations to the pn knockout has to compete with a significant contribution from pion exchange currents [6–14]. Furthermore, one has to treat the tensor correlations appropriately. It is the aim of this investigation to employ correlated many-body wave functions, which are derived from a realistic NN interaction, in a calculation of $(e, e'pn)$ cross sections which accounts for the contribution of one- and two-body parts in the nuclear current operator.

The correlated wave functions are determined in the framework of the coupled cluster method, which is also often referred to as the $\text{exp}(S)$ method [15–19], using the so-called S_2 approximation. This approach is similar to the evaluation of the two-body spectral function in terms of the Brueckner G -matrix as it has been used e.g. in the analysis of the $^{16}\text{O}(e, e'pp)^{14}\text{C}$ reaction [2,4,20]. The Argonne V14 potential [21] has been used for the NN interaction.

After this introduction we will shortly review the coupled cluster method in section 2 and discuss some features of the correlated wave functions derived in this scheme. The calculation of the matrix elements for the one- and two-body current contributions and the resulting cross sections are described in section 3. After the discussion of the numerical results for the $^{16}\text{O}(e,e'pn)^{14}\text{N}$ reaction in section 4, we will summarize our main results and conclusions.

II. CORRELATED NN WAVE FUNCTIONS IN THE COUPLED CLUSTER METHOD

The basic features of the coupled cluster method have been described already in the review article by Kümmel et al. [15]. More recent developments and applications can be found in [17]. Here we will only present some basic equations, which are necessary to describe the approach we have used to determine the correlated nuclear wave functions to be used in the calculation of cross sections for the exclusive $^{16}\text{O}(e,e'pn)^{14}\text{N}$ reaction. The many-body wave function of the coupled cluster or $\exp(S)$ method can be written

$$|\Psi\rangle = \exp\left(\sum_{n=1}^A \hat{S}_n\right) |\Phi\rangle. \quad (1)$$

The state $|\Phi\rangle$ refers to the uncorrelated model state, which we have chosen to be a Slater determinant of harmonic oscillator functions with an oscillator length $b=1.72$ fm, which is appropriate for the description of our target nucleus ^{16}O . This choice leads to small amplitudes for the operator S_1 . The linked n -particle n -hole excitation operators can be written

$$\hat{S}_n = \frac{1}{n!2} \sum_{\nu_i \rho_i} \langle \rho_1 \dots \rho_n | S_n | \nu_1 \dots \nu_n \rangle a_{\rho_1}^\dagger \dots a_{\rho_n}^\dagger a_{\nu_n} \dots a_{\nu_1}. \quad (2)$$

Here and in the following the sum is restricted to oscillator states ρ_i which are unoccupied in the model state $|\Phi\rangle$, while states ν_i refer to states which are occupied in $|\Phi\rangle$. For the application discussed here we assume the so-called S_2 approximation, i.e. we restrict the correlation operator in (1) to the terms with \hat{S}_1 and \hat{S}_2 . One may introduce one- and two-body wave functions

$$\begin{aligned} \psi_1 |\nu_1\rangle &= |\nu_1\rangle + \hat{S}_1 |\nu_1\rangle \\ \psi_2 |\nu_1 \nu_2\rangle &= \mathcal{A} \psi_1 |\nu_1\rangle + \psi_1 |\nu_2\rangle + \hat{S}_2 |\nu_1 \nu_2\rangle \end{aligned} \quad (3)$$

with \mathcal{A} denoting the operator antisymmetrizing the product of one-body wave functions. Using these definitions one can write the coupled equations for the evaluation of the correlation operators \hat{S}_1 and \hat{S}_2 in the form

$$\langle \alpha | \hat{T}_1 \psi_1 | \nu \rangle + \sum_{\nu_1} \langle \alpha \nu_1 | \hat{T}_2 \hat{S}_2 + \hat{V}_{12} | \nu \nu_1 \rangle = \sum_{\nu_1} \epsilon_{\nu_1 \nu} \langle \alpha | \psi_1 | \nu_1 \rangle, \quad (4)$$

where \hat{T}_i stands for the operator of the kinetic energy of particle i and \hat{V}_{12} is the two-body potential. Furthermore we introduce the single-particle energy matrix defined by

$$\epsilon_{\nu_1 \nu} = \langle \nu_1 | \hat{T}_1 | \nu \rangle + \sum_{\nu'} \langle \nu_1 \nu' | \hat{V}_{12} \psi_2 | \nu \nu' \rangle \quad (5)$$

The Hartree-Fock type equation (4) is coupled to a two-particle equation of the form

$$\begin{aligned} 0 = & \langle \alpha \beta | \hat{Q} \left[(\hat{T}_1 + \hat{T}_2) \hat{S}_2 + \hat{V}_{12} \psi_2 + \hat{S}_2 \hat{P} \hat{V}_{12} \psi_2 \right] | \nu_1 \nu_2 \rangle \\ & - \sum_{\nu} \left(\langle \alpha \beta | \hat{S}_2 | \nu \nu_2 \rangle + \epsilon_{\nu \nu_1} + \langle \alpha \beta | \hat{S}_2 | \nu_1 \nu \rangle + \epsilon_{\nu \nu_2} \right) \end{aligned} \quad (6)$$

In this equation we have introduced the Pauli operator \hat{Q} projecting on two-particle states, which are not occupied in the uncorrelated model state $|\Phi\rangle$ and the projection operator \hat{P} , which projects on two-particle states, which are occupied. If for a moment we ignore the term in (4) which is represented by the operators $\hat{T}_2 \hat{S}_2$ and also the term in (6) characterized by the operator $\hat{S}_2 \hat{P} \hat{V}_{12}$ the solution of these coupled equations corresponds to the Brueckner-Hartree-Fock approximation and we can identify the matrix elements of $\hat{V}_{12} \psi_2$ with the Brueckner G -matrix. Indeed

the effects of these two terms are rather small and we have chosen the coupled cluster approach mainly because it provides directly correlated two-body wave functions.

The coupled equations (4) and (6) have been solved by expanding the amplitudes defining S_2 and the wave functions ψ_2 in terms of product wave functions for the relative and center of mass coordinates

$$\mathbf{r}_{12} = \mathbf{r}_1 - \mathbf{r}_2, \quad \mathbf{R} = \frac{\mathbf{r}_1 + \mathbf{r}_2}{2} \quad (7)$$

The harmonic oscillator wave functions corresponding to the model state $|\Phi\rangle$ turn out to provide a useful basis for the center of mass wave functions, while the relative wave functions are represented more efficiently in a complete basis of eigenstates for a spherical box of radius r_{\max} . It turns out that the results are independent on the choice of r_{\max} if this value is chosen large enough as compared to the relative distances between two nucleons in ^{16}O ($r_{\max} \approx 10$ fm or larger) [19].

This means that we can write the correlated two-body wave functions with σ_i denoting the spin and J referring to the total angular momentum of the pair

$$\begin{aligned} \langle \mathbf{r}_{12}, \mathbf{R}, \boldsymbol{\sigma}_1, \boldsymbol{\sigma}_2 | \psi_2 | \nu_1 \nu_2 \rangle_J &= \sum_{lSjNL} c_{lSjNL}^{\nu_1 \nu_2 J} \phi_{lSjNL}^{\nu_1 \nu_2 J}(r_{12}) R_{NL}(R) \\ &\times \left[\mathfrak{S}_{lS}^j(\Omega_r, \boldsymbol{\sigma}_1, \boldsymbol{\sigma}_2) Y_L(\Omega_R) \right]^J, \end{aligned} \quad (8)$$

If we would ignore all correlation effects, this equation corresponds to the Talmi-Moshinsky transformation of harmonic oscillator states from the laboratory frame (oscillator states ν_1 and ν_2) to relative and center of mass coordinates. In this case the eq. (8) is simplified. The relative wave functions $\phi_{lSjNL}^{\nu_1 \nu_2 J}$ do not depend on the quantum numbers S, j, N, L, ν_1, ν_2 and J and are simply given in terms of harmonic oscillator functions. The coefficients $c_{lSjNL}^{\nu_1 \nu_2 J}$ are the well known coefficients of the Talmi-Moshinsky transformation and are different from zero only if the oscillator relation

$$2n + l + 2N + L = 2n_1 + l_1 + 2n_2 + l_2$$

holds, with n_i, l_i referring to oscillator quantum numbers of state ν_i .

In order to visualize the effects of NN correlations we would like to discuss a specific example, a proton and a neutron in $p_{1/2}$ shell coupled to $J = 1$. The non-vanishing Talmi-Moshinsky transformation coefficients are given by

$$\begin{aligned} &\sqrt{\frac{1}{54}}, \text{ for } {}^3S_1, N = L = 0 \\ &-\sqrt{\frac{10}{27}}, \text{ for } {}^3D_1, N = L = 0 \\ &\sqrt{\frac{10}{27}}, \text{ for } {}^3S_1, N = 0, L = 2 \\ &-\sqrt{\frac{1}{54}}, \text{ for } {}^3S_1, N = 1, L = 0 \\ &\sqrt{\frac{6}{27}}, \text{ for } {}^1P_1, N = 0, L = 1. \end{aligned} \quad (9)$$

The relative wave functions, calculated with the Argonne V14 potential, for some of these channels are displayed in Fig. 1. In the case of the uncorrelated approach (dashed lines) these wave functions are simply given by the corresponding harmonic oscillator functions multiplied with one of the Talmi-Moshinsky transformation coefficients listed in (9). The correlated wave functions, however, show different shapes. At small relative distances r the amplitudes for the 3S_1 partial waves are typically smaller than for the corresponding uncorrelated wave, reflecting the repulsive interaction at such small distances. For larger distances the correlated wave function approach the uncorrelated ones (healing property). Note, that correlated wave functions are also obtained for channels like the ${}^3D_1, N = 0, L = 2$, for which the uncorrelated wave function vanishes. These are mainly due to the tensor correlations. It is also worth mentioning that our approach yields state-dependent correlation functions in the sense that the correlated wave functions $\phi_{lSjNL}^{\nu_1 \nu_2 J}$ depend on all quantum numbers which are attached as sub- or superscript. This state dependence can be seen in the examples displayed in Fig. 1.

III. CROSS SECTION AND REACTION MECHANISM

The coincidence cross section for the reaction induced by an electron with momentum \mathbf{p}_0 and energy E_0 , with $E_0 = |\mathbf{p}_0| = p_0$, where two nucleons, with momenta \mathbf{p}'_1 , and \mathbf{p}'_2 and energies E'_1 and E'_2 , are ejected from a nucleus is given, in the one-photon exchange approximation and after integrating over E'_2 , by [6,22]

$$\frac{d^8\sigma}{dE'_0 d\Omega dE'_1 d\Omega'_1 d\Omega'_2} = K \Omega_f f_{\text{rec}} |j_\mu J^\mu|^2. \quad (10)$$

In Eq. (10) E'_0 is the energy of the scattered electron with momentum \mathbf{p}'_0 , $K = e^4 p_0'^2 / 4\pi^2 Q^4$ where $Q^2 = \mathbf{q}^2 - \omega^2$, with $\omega = E_0 - E'_0$ and $\mathbf{q} = \mathbf{p}_0 - \mathbf{p}'_0$, is the four-momentum transfer. The quantity $\Omega_f = p'_1 E'_1 p'_2 E'_2$ is the phase-space factor and integration over E'_2 produces the recoil factor

$$f_{\text{rec}}^{-1} = 1 - \frac{E'_2}{E_B} \frac{\mathbf{p}'_2 \cdot \mathbf{p}_B}{|\mathbf{p}'_2|^2}, \quad (11)$$

where E_B and \mathbf{p}_B are the energy and momentum of the residual nucleus. The cross section is given by the square of the scalar product of the relativistic electron current j^μ and of the nuclear current J^μ , which is given by the Fourier transform of the transition matrix elements of the charge-current density operator between initial and final nuclear states

$$J^\mu(\mathbf{q}) = \int \langle \Psi_f | \hat{J}^\mu(\mathbf{r}) | \Psi_i \rangle e^{i\mathbf{q} \cdot \mathbf{r}} d\mathbf{r}. \quad (12)$$

If the residual nucleus is left in a discrete eigenstate of its Hamiltonian, i.e. for an exclusive process, and under the assumption of a direct knockout mechanism, Eq. (12) can be written as [22,23]

$$J^\mu(\mathbf{q}) = \int \psi_f^*(\mathbf{r}_1 \boldsymbol{\sigma}_1, \mathbf{r}_2 \boldsymbol{\sigma}_2) J^\mu(\mathbf{r}, \mathbf{r}_1 \boldsymbol{\sigma}_1, \mathbf{r}_2 \boldsymbol{\sigma}_2) \psi_i(\mathbf{r}_1 \boldsymbol{\sigma}_1, \mathbf{r}_2 \boldsymbol{\sigma}_2) \times e^{i\mathbf{q} \cdot \mathbf{r}} d\mathbf{r} d\mathbf{r}_1 d\mathbf{r}_2 d\boldsymbol{\sigma}_1 d\boldsymbol{\sigma}_2. \quad (13)$$

Eq. (13) contains three main ingredients: the two-nucleon overlap integral ψ_i , the nuclear current J^μ and the final-state wave function ψ_f .

In the model calculations the final-state wave function ψ_f includes the interaction of each one of the two outgoing nucleons with the residual nucleus while their mutual interaction is neglected. Therefore, the scattering state is written as the product of two uncoupled single-particle distorted wave functions, eigenfunctions of a complex phenomenological optical potential which contains a central, a Coulomb and a spin-orbit term.

The nuclear current operator in Eq. (13) is the sum of a one-body and a two-body part. In the one-body part convective and spin currents are included. The two-body current is derived from the effective Lagrangian of ref. [9], performing a non relativistic reduction of the lowest-order Feynman diagrams with one-pion exchange. We have thus currents corresponding to the seagull and pion-in-flight diagrams and to the diagrams with intermediate isobar configurations [10], i.e.

$$\mathbf{J}^{(2)}(\mathbf{r}, \mathbf{r}_1 \boldsymbol{\sigma}_1, \mathbf{r}_2 \boldsymbol{\sigma}_2) = \mathbf{J}^{\text{sea}}(\mathbf{r}, \mathbf{r}_1 \boldsymbol{\sigma}_1, \mathbf{r}_2 \boldsymbol{\sigma}_2) + \mathbf{J}^\pi(\mathbf{r}, \mathbf{r}_1 \boldsymbol{\sigma}_1, \mathbf{r}_2 \boldsymbol{\sigma}_2) + \mathbf{J}^\Delta(\mathbf{r}, \mathbf{r}_1 \boldsymbol{\sigma}_1, \mathbf{r}_2 \boldsymbol{\sigma}_2). \quad (14)$$

Details of the nuclear current components and the values of the parameters used in the calculations are given in Ref. [10].

The two-nucleon overlap integral ψ_i contains the information on nuclear structure and allows one to write the cross section in terms of the two-hole spectral function [6]. For a discrete final state of the ^{14}N nucleus, with angular momentum quantum number J , the state ψ_i is expanded in terms of the two-hole wave functions defined in (8) as

$$\psi_i^J(\mathbf{r}_1 \boldsymbol{\sigma}_1, \mathbf{r}_2 \boldsymbol{\sigma}_2) = \sum_{\nu_1 \nu_2} a_{\nu_1 \nu_2}^J \langle \mathbf{r}_{12}, \mathbf{R}, \boldsymbol{\sigma}_1, \boldsymbol{\sigma}_2 | \psi_2 | \nu_1 \nu_2 \rangle \quad (15)$$

The expansion coefficients $a_{\nu_1 \nu_2}^J$ are determined from a configuration mixing calculation of the two-hole states in ^{16}O , which can be coupled to the angular momentum and parity of the requested state. The residual interaction for this shell-model calculation is also derived from the Argonne V14 potential and corresponds to the Brueckner G-matrix. The expansion coefficients $a_{\nu_1 \nu_2}^J$, given in Table I for the transitions to the low-lying states of ^{14}N considered in this paper, are renormalized to account for the spectroscopic factors of the single-particle states as it is described in [20].

IV. THE $^{16}\text{O}(e,e'\text{pn})^{14}\text{N}$ KNOCKOUT REACTION TO DISCRETE FINAL STATES

In this section we present numerical results of the cross section of the $^{16}\text{O}(e,e'\text{pn})^{14}\text{N}$ reaction for transitions to the lowest-lying discrete states in the residual nucleus that are expected to be strongly populated by direct knockout. We consider three states, all of them with positive parity and $T = 0$: the 1_1^+ ground state of ^{14}N , the 1_2^+ state at 3.95 MeV and the 2^+ state at 7.03 MeV. These states are of particular interest for our investigation since they can be separated in high-resolution experiments such as that recently proposed at MAMI [5]. The configuration mixing calculations described at the end of section 3 predict excitation energies of 4.54 MeV for the 1_2^+ and 7.17 MeV for the 2^+ state.

In the calculations each state is characterized by a particular value of the missing energy, given by

$$E_{2m} = \omega - T_1' - T_2' - T_B = E_s + E_x, \quad (16)$$

where T_1' , T_2' and T_B are the kinetic energies of the two outgoing nucleons and of the residual nucleus, respectively, E_s is the separation energy at threshold for two-nucleon emission and E_x is the excitation energy of the residual nucleus.

As an example, we have performed calculations in the so-called super-parallel kinematics [22], where the knocked-out nucleons are detected parallel and anti-parallel to the transferred momentum \mathbf{q} . In this kinematics, for a fixed value of the energy and momentum transfer and for a particular final state, it is possible to explore, for different values of the kinetic energies of the outgoing nucleons, all possible values of the recoil (p_B) or missing momentum (p_{2m}) distribution, where

$$\mathbf{p}_{2m} = \mathbf{p}_B = \mathbf{q} - \mathbf{p}'_1 - \mathbf{p}'_2. \quad (17)$$

The super-parallel kinematics is favored by the fact that only two structure functions, the longitudinal and transverse structure functions, contribute to the cross section, as in the inclusive electron scattering, and, as in that case, can in principle be separated by a Rosenbluth plot [22]. This kinematical setting is also favorable from the experimental point of view. It has been realized in a recent $^{16}\text{O}(e,e'\text{pp})^{14}\text{C}$ experiment at MAMI [3] and has been proposed for the first experimental study of the $^{16}\text{O}(e,e'\text{pn})^{14}\text{N}$ reaction [5]. The choice of the same kinematics is of particular interest for the comparison of cross sections and reaction mechanisms for pp and pn emission, for the investigation of the relative strength of pp and pn correlations and of their contributions in the two processes and for the determination of both types of correlations.

The same kinematical parameters of the MAMI experiment have been adopted in the calculations, with $E_0 = 855$ MeV, electron scattering angle $\theta = 18^\circ$, $\omega = 215$ MeV and $q = 316$ MeV/ c . The proton is emitted parallel and the neutron antiparallel to the momentum transfer \mathbf{q} . This choice appears well suited to reduce the contribution of meson-exchange currents and emphasize effects due to correlations [24].

The cross section for the transition to the 1_1^+ ground state of ^{14}N is shown in Fig. 2. Separate contributions of the different terms of the nuclear current are shown in the figure and compared with the total cross section. The contribution of the one-body current, entirely due to correlations, is large. It is of the same size as that of the pion seagull current. The contribution of the Δ -current is much smaller at lower values of p_B , whereas for values of p_B larger than 100 MeV/ c it becomes comparable with that of the other components. The contribution of the pion-in-flight current is generally much smaller, but at higher values of the recoil momentum. The final result indicates that all the terms of the nuclear current give a significant contribution to the calculated cross section and that interference effects are not too large. The major role is played in the considered situation by the 1-body and seagull terms. In particular, the one-body current and thus correlations yield a contribution that is important to determine the size and the shape of the cross section.

The shape of the recoil-momentum distribution is driven by the c.m. orbital angular momentum L of the knocked out pair. This feature, that is fulfilled in a factorized approach [25], where final-state interaction is neglected and \mathbf{p}_B is opposite to the total momentum of the initial nucleon pair, is not spoiled in an unfactorized approach by final-state interaction [4,10,23].

Different partial waves of relative and c.m. motion contribute to the two-nucleon overlap function in Eqs. (15) and (8). Each transition is thus characterized by different components, with specific values of L (see Section 2), whose relative weights will determine the shape of the recoil momentum distribution. This can be seen in Fig. 3, where the separate contributions of the different partial waves of relative motion are displayed. For the transition to the 1_1^+ ground state there are the following relative states: 3S_1 , combined with a c.m. $L = 0$ and $L = 2$, 1P_1 , combined with $L = 1$, and 3D_1 . For the 3D_1 relative wave function we have separated in the figure the component already present in the uncorrelated wave function, which is combined with $L = 0$, and the component produced by tensor correlations and not present in the uncorrelated wave function, which is combined with $L = 0$ and $L = 2$ (see also Fig. 1 and discussion above). In the following we will call these two terms 3D_1 and $^3D_1^T$, respectively. The contribution of the

${}^3D_1^T$ partial wave emphasizes the relevant role played in the calculations by tensor correlations, which are however present and important also in the other components.

In Fig. 3 the shapes of the recoil-momentum distributions for the different relative states are basically determined by the value of L , since final-state interaction modifies the momentum of the pair but does not change drastically the shape. The shape of the final cross section is driven by the component which gives the major contribution, i.e. for the 1_1^+ state and in the considered kinematics by 3S_1 . An important, although less relevant role, is also played by ${}^3D_1^T$, mainly at large values of p_B , while 3D_1 is less important and 1P_1 is practically negligible. The final cross section is thus a combination of states with $L = 0$ and $L = 2$. For low values of p_B it has a typical s -wave shape, while at large values of p_B the d -wave contribution prevails.

The dependence of the cross sections calculated for different relative states on the various components of the nuclear current is displayed in Fig. 4. Two-body currents and correlations play a different role in 3S_1 and 3D_1 knockout. The seagull and Δ -isobar currents give the major contribution to 3S_1 . Here the one-body current is not too relevant, although non negligible. In contrast, it is much more important in 3D_1 , where it is dominant, and in ${}^3D_1^T$, where the contributions of the one-body and Δ currents are of about the same size and add up in the cross section. Two-body currents give the major contribution also to 1P_1 , but the role of this relative wave in the cross section is very small.

The major contribution to the total cross section is thus given by 3S_1 and to a lesser extent also by ${}^3D_1^T$. The relevant role played by correlations in ${}^3D_1^T$, which is determined by tensor correlations, and in 3D_1 is therefore the main responsible for the important effect of the one-body current in the cross section of Fig. 2.

In Fig. 5 the same quantities as in Fig. 2 are shown, but the two-nucleon overlap has been calculated with the simpler prescription of ref. [10], i.e. by the product of the pair function of the shell model, described for 1_1^+ as a pure $(p_{1/2})^{-2}$ hole, and of a Jastrow type central and state independent correlation function.

The large differences between the cross sections in Figs. 2 and 5 indicate that a refined description of the two-nucleon overlap, involving a careful treatment of both aspects related to nuclear structure and NN correlations, is needed to give reliable predictions of the size and the shape of the $(e,e'pn)$ cross section. This result, that is well established for the $(e,e'pp)$ reaction also in comparison with data [2–4], is here confirmed also for the $(e,e'pn)$ reaction. In particular, the calculated cross sections are very sensitive to the treatment of NN correlations. The difference between the results in Figs. 2 and 5 is indeed dramatic for the separate contribution of the one-body current, which is completely determined by correlations. This contribution, that in Fig. 2 is competitive with or even larger than that of the two-body current, is negligible in Fig. 5. The correlation function adopted in Fig. 5 neglects the difference between pp and np correlations and their state dependence. Moreover, it does not take into account tensor correlations, which are crucial in the pn channel. Therefore, this treatment represents a too simple prescription, that is not able to give a proper description of correlations effects in the $(e,e'pn)$ cross section. The contribution of the two-body current, which is expected to be generally very important or even dominant in pn knockout, is also expected to be much less affected by correlations and thus by their treatment. The comparison between Figs. 2 and 5 indicate, however, that the model used for the two-nucleon overlap function has meaningful effects also on the various terms of the two-body current. These effects are of course less dramatic than those obtained on the one-body current, but are anyhow large.

The comparison between Figs. 2 and 5 is only an example, but it clearly shows that reliable numerical predictions of the $(e,e'pn)$ cross section require a careful description of the two-nucleon overlap functions involving a refined and consistent treatment of long-range and short-range correlations.

The cross sections for the transition to the 1_2^+ state are displayed in Figs. 6 and 7. The two-nucleon overlap function for this state contains the same components in terms of relative and c.m. wave functions and the same defect functions as for the 1_1^+ ground state, but they are weighed with different amplitudes $a_{\nu_1\nu_2}^J$ in Eq. (15). In practice the two overlap functions have different amplitudes for $p_{1/2}$ and $p_{3/2}$ holes (see Table I). This has the consequence that the cross sections in Figs. 2 and 6 have a different shape and are differently affected by the various terms of the nuclear current. The shape of the recoil-momentum distribution in Fig. 6 indicates a more prominent role of the components with c.m. $L = 2$. The comparison between the contributions of the different terms of the nuclear current in the two states shows that the Δ -current, which in Fig. 2 for 1_1^+ is much less important than the one-body and seagull terms, is much larger and even dominant in the 1_2^+ state. In contrast, the one-body and seagull currents, that play the main role for the transition to the ground state, are less important for 1_2^+ . The one-body current gives a meaningful contribution only for recoil momenta between 100 and 200 MeV/c. The contribution of the seagull current is generally small and that of the pion-in-flight current is even smaller. This result can better be understood in Fig. 7, where separate contributions of the relative waves and their dependence on the terms of the nuclear current are displayed. There are two main differences between the cross sections in Figs. 4 and 7: the different role played by 3S_1 and 3D_1 , and the dominant contribution of the Δ -current in 3D_1 knockout. The 3D_1 relative wave function in Fig. 7 is much more important than for the transition to the 1_1^+ state and gives the major contribution to the cross section. However, while in the corresponding situation for the 1_1^+ state it is dominated by the one-body current, in 1_2^+ it is dominated by the Δ -current. Moreover, the Δ -current is for this transition more important also in ${}^3D_1^T$ knockout. It is less meaningful in 3S_1 , but the role of this relative state in the final cross section is less relevant for the 1_2^+ than for the

1_1^+ state. Thus, the major contribution to the final cross section is given by the Δ -current.

All the three states 3S_1 , 3D_1 and ${}^3D_1^T$ play a significant role in the cross section, while 1P_1 is negligible also for the 1_2^+ state. The comparison between the shapes of the recoil momentum distributions of 3S_1 knockout in Figs. 4 and 7 indicates a more prominent role of the components with c.m. $L = 2$ for the 1_2^+ state. This feature, which is more evident at large values of the recoil momentum, explains the shape of the final cross section in Fig. 6.

The results for the transition to the 2^+ state are displayed in Figs. 8 and 9. The shape of the recoil-momentum distribution for this transition is different from that of the other states previously considered. The position of the maximum at $p_B \simeq 200$ MeV/c is an indication of the relevant contribution of the partial wave functions with c.m. $L = 2$. The Δ -current dominates with respect to the other terms in the maximum region, whereas at low values of the recoil momentum all the three terms, Δ seagull and one-body, contribute with similar weights. The contribution of the pion-in-flight current is always very small.

The separate cross sections produced by different partial waves of relative motion are displayed in Fig. 9. For this final state they are: 3S_1 , which is combined with $L = 0$ and $L = 2$, 3D_2 , combined with $L = 0$, and 3D_1 , not present in the uncorrelated wave function and produced by tensor correlations, which is also combined with $L = 0$ and $L = 2$. The components with $L = 0$ prevail at low values of p_B , where they give a contribution of about the same size for all the three relative states. The components with $L = 2$, present only in 3D_1 and 3S_1 , are dominant at large values of the recoil momentum. In 3S_1 all the different terms of the nuclear current, including pion-in-flight, give a meaningful contribution to the cross section. In 3D_2 the role of pion-in-flight is negligible, but the other terms all give a meaningful contribution. In 3D_1 the cross sections calculated with the one-body and Δ currents are of about the same size, whereas those calculated with seagull and pion-in-flight are much smaller. The Δ -current is therefore important in all the three relative states, in particular at large values of the recoil momentum, while the one-body current gives a more meaningful contribution to 3D_1 and 3D_2 knockout and at low values of p_B .

V. SUMMARY AND CONCLUSIONS

The cross section has been calculated for the ${}^{16}\text{O}(e,e'\text{pn}){}^{14}\text{N}$ reaction leading to the ground state and the first excited 1^+ and 2^+ states in the residual nucleus ${}^{14}\text{N}$. The calculations account for correlation effects, using correlated wave functions calculated in the framework of the coupled cluster method, MEC contributions and the effects of final state interaction of the outgoing nucleons with the residual nucleus. As an example we consider the so-called super-parallel kinematics with a value for the energy ($\omega = 215$ MeV) and momentum transfer ($q = 316$ MeV/c) which is appropriate for experiments to be performed at MAMI in Mainz. The cross sections for $(e,e'\text{pn})$ are about an order of magnitude larger than corresponding cross sections for $(e,e'\text{pp})$ reactions. This enhancement is partly due to the importance of MEC, the pion seagull contribution in particular, and partly due to the enhanced importance of correlation effects in pn pairs as compared to pp pairs. The relative importance of the MEC contribution as compared to the correlation effects depends on the final state of the residual nucleus. This is similar to the observations made for $(e,e'\text{pp})$ [4]. The calculated cross sections are rather sensitive to details of the nuclear correlations considered and in particular to the presence of the tensor component. In fact, a correlation function without this component gives quite different results for the calculated cross sections. Also the choice of the structure amplitudes is important and produces a sensible effect in the shape and size of the cross sections. This means that an accurate determination of the spectral density and therefore of the overlap wave functions is required in order to predict in a satisfactory and reliable way the experimental yields. This will hopefully enable us to disentangle the effects of the MEC contributions from those of the nuclear correlations. These observations support the efforts to complete our knowledge on nuclear correlations obtained from $(e,e'\text{pp})$ reactions by corresponding experiments on $(e,e'\text{pn})$.

These investigations have partly been supported by the Deutsche Forschungsgemeinschaft (“Schwerpunktprogramm, WA 728/3”).

[1] C. J. G. Onderwater, K. Allaart, E. C. Aschenauer, Th. S. Bauer, D. J. Boersma, E. Cisbani, S. Frullani, F. Garibaldi, W. J. W. Geurts, D. Groep, W. H. A. Hesselink, M. Iodice, E. Jans, N. Kalantar-Nayestanaki, W. -J. Kasdorp, C. Kormanyos, L. Lapikás, J. J. van Leeuwe, R. De Leo, A. Misiejuk, A. R. Pellegrino, R. Perrino, R. Starink, M. Steenbakkens, G. van der Steenhoven, J. J. M. Steijger, M. A. van Uden, G. M. Urciuoli, L. B. Weinstein, and H. W. Willering, *Phys. Rev. Lett.* **78**, 4893 (1997).

- [2] C. J. G. Onderwater, K. Allaart, E. C. Aschenauer, Th. S. Bauer, D. J. Boersma, E. Cisbani, W. H. Dickhoff, S. Frullani, F. Garibaldi, W. J. W. Geurts, C. Giusti, D. Groep, W. H. A. Hesselink, M. Iodice, E. Jans, N. Kalantar-Nayestanaki, W. - J. Kasdorp, C. Kormanyos, L. Lapikás, J. J. van Leeuwe, R. De Leo, A. Misiejuk, H. Müther, F. D. Pacati, A. R. Pellegrino, R. Perrino, R. Starink, M. Steenbakkens, G. van der Steenhoven, J. J. M. Steijger, M. A. van Uden, G. M. Urciuoli, L. B. Weinstein, and H. W. Willering, *Phys. Rev. Lett.* **81**, 2213 (1998).
- [3] G. Rosner, *Conference on Perspectives in Hadronic Physics*, eds. S. Boffi, C. Ciofi degli Atti, and M. M. Giannini (World Scientific, Singapore, 1998) p.185;
Proceedings of the 10th Mini-Conference on Studies of Few-Body Systems with High Duty-Factor Electron Beams, NIKHEF, Amsterdam 1999, in press
- [4] C. Giusti, F. D. Pacati, K. Allaart, W. J. W. Geurts, W. H. Dickhoff and H. Müther, *Phys. Rev. C* **57**, 1691 (1998).
- [5] J. R. M. Annand, P. Bartsch, D. Baumann, J. Becker, R. Böhm, D. Branford, S. Derber, M. Ding, I. Ewald, K. Föhl, J. Friedrich, J. M. Friedrich, P. Grabmayr (spokesperson), T. Hehl, D. G. Ireland, P. Jennewein, M. Kahrau, D. Knödler, K. W. Krygier, A. Liesenfeld, I. J. D. MacGregor, H. Merkel, K. Merle, P. Merle, U. Müller, H. Müther, A. Natter, R. Neuhausen, Th. Pospischil, G. Rosner (spokesperson), H. Schmieden, A. Wagner, G. J. Wagner, Th. Walcher, M. Weis, S. Wolf, MAMI proposal Nr: A1/5-98.
- [6] S. Boffi, C. Giusti, F. D. Pacati and M. Radici, *Electromagnetic Response of Atomic Nuclei*, Oxford Studies in Nuclear Physics (Clarendon Press, Oxford, 1996).
- [7] J.-F. Mathiot, *Phys. Rep.* **173**, 64 (1989).
- [8] D. O. Riska, *Phys. Rep.* **181**, 208 (1989).
- [9] R. D. Peccei, *Phys. Rev.* **176**, 1812 (1968); **181**, 1902 (1969).
- [10] C. Giusti and F. D. Pacati, *Nucl. Phys.* **A641**, 297 (1998).
- [11] M. Vanderhaeghen, L. Machenil, J. Ryckebusch, and M. Waroquier, *Nucl. Phys. A* **580**, 551 (1994).
- [12] L. Machenil, M. Vanderhaeghen, J. Ryckebusch, and M. Waroquier, *Phys. Lett. B* **316**, 17 (1993).
- [13] J. Ryckebusch, V. Van der Sluys, K. Heyde, H. Holvoet, W. Van Nespren and M. Waroquier, *Nucl. Phys. A* **624**, 581 (1997).
- [14] P. Wilhelm, H. Arenhövel, C. Giusti, and F. D. Pacati, *Z. Phys. A* **359**, 467 (1997).
- [15] H. Kümmel, K. H. Lührmann, and J. G. Zabolitzky, *Phys. Rep.* **36**, 1 (1978).
- [16] J. G. Zabolitzky, *Nucl. Phys.* **A228**, 272 (1974).
- [17] R. F. Bishop, in *Microscopic Quantum Many-Body Theories and Their Applications*, eds. J. Navarro and A. Polls (Springer 1998).
- [18] J. H. Heisenberg and B. Mihaila, nucl-th/9802029.
- [19] M. Stauf, diploma thesis (University of Tübingen, 1998).
- [20] W. J. W. Geurts, K. Allaart, W. H. Dickhoff and H. Müther, *Phys. Rev. C* **54**, 1144 (1996).
- [21] R. B. Wiringa, R. A. Smith, and T. L. Ainsworth, *Phys. Rev. C* **29**, 1207 (1984).
- [22] C. Giusti and F. D. Pacati, *Nucl. Phys.* **A535**, 573 (1991);
Nucl. Phys. **A571**, 694 (1994).
- [23] C. Giusti and F. D. Pacati, *Nucl. Phys.* **A615**, 373 (1997).
- [24] D. Knödler and H. Müther, preprint Los Alamos archive nucl-th/9812047.
- [25] K. Gottfried, *Nucl. Phys.* **5**, 557 (1958).
- [26] A. Nadasen, P. Schwandt, P. P. Singh, W. W. Jacobs, A. D. Bacher, P. T. Debevec, M. D. Kaichuk and J. T. Meek, *Phys. Rev. C* **23**, 1023 (1981).
- [27] L. R. B. Elton and A. Swift, *Nucl. Phys.* **A94**, 52 (1967).
- [28] C. C. Gearhart, Ph.D thesis, Washington University, St. Louis (1994);
C. C. Gearhart, and W. H. Dickhoff, private communication.

J^π	$(p_{3/2})^{-2}$	$(p_{3/2}p_{1/2})^{-1}$	$(p_{1/2})^{-2}$
1_1^+	0.070	-0.455	0.606
1_2^+	0.271	-0.544	-0.460
2^+	0.	0.765	0.

TABLE I. The coefficients $a_{\nu_1\nu_2}^J$ in Eq. (15) for the low-lying states of ^{14}N .

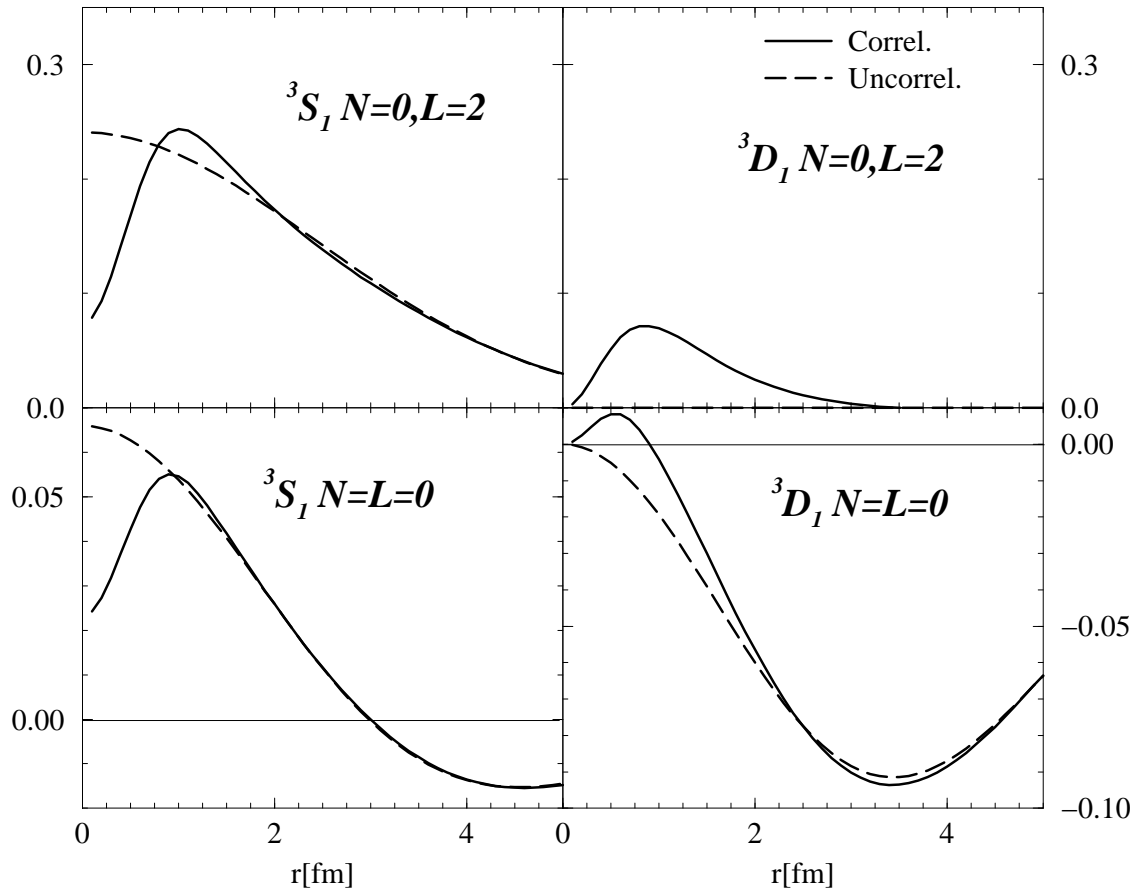


FIG. 1. Relative wave functions for correlated and uncorrelated two-body wave functions in the case of a proton and a neutron in the $p_{1/2}$ shell coupled to $J = 1$. Further discussion in the text.

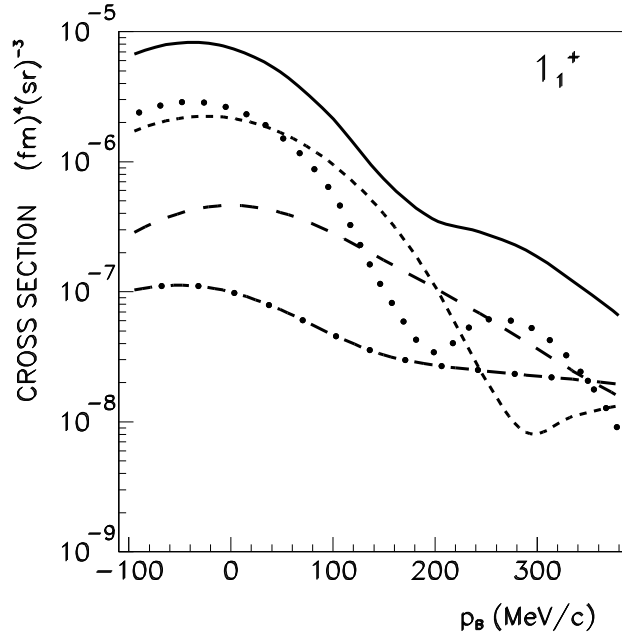


FIG. 2. The differential cross section of the $^{16}\text{O}(e,e'pn)$ reaction as a function of the recoil momentum p_B for the transition to the 1_1^+ ground state of ^{14}N ($E_{2m} = 22.96$ MeV), in the super-parallel kinematics with $E_0 = 855$ MeV, and $\omega = 215$ MeV $q = 316$ MeV/ c . The recoil-momentum distribution is obtained changing the kinetic energies of the outgoing nucleons. Separate contributions of the one-body, seagull, pion-in-flight and Δ -current are shown by the dotted, short-dashed, dot-dashed and long-dashed lines, respectively. The solid line gives the total cross section. The optical potential is taken from Ref. [26]. Positive (negative) values of p_B refer to situations where \mathbf{p}_B is parallel (antiparallel) to \mathbf{q} .

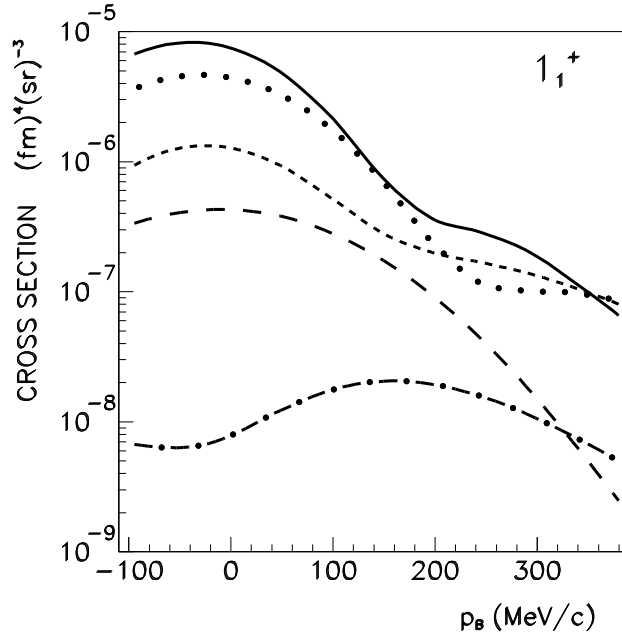


FIG. 3. The differential cross section of the $^{16}\text{O}(e,e'pn)$ reaction as a function of the recoil momentum p_B for the same transition and in the same kinematics as in Fig. 2. Optical potential as in Fig. 2. Separate contributions of different partial waves of relative motions are drawn: dotted line for 3S_1 , dot-dashed line for 1P_1 , short-dashed line gives the 3D_1 component already present in the uncorrelated wave function and long-dashed line the 3D_1 component due to tensor correlations. The solid line is the same as in Fig. 2.

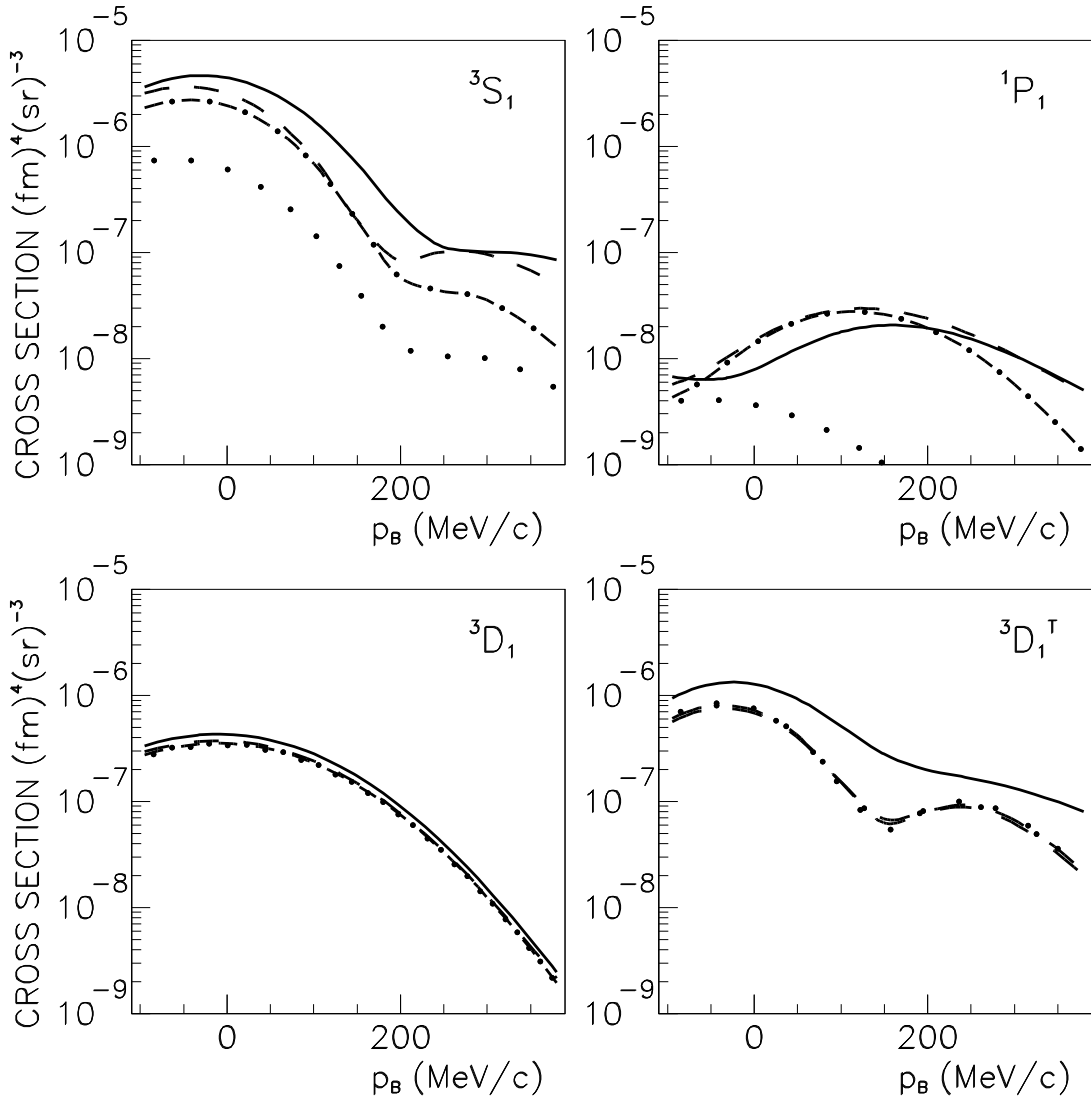


FIG. 4. The differential cross section of the $^{16}\text{O}(e,e'pn)$ reaction as a function of the recoil momentum p_B for the same transition and in the same kinematics as in Fig. 2. Optical potential as in Fig. 2. Separate contributions of different partial waves of relative motions are drawn: 3S_1 , 1P_1 , 3D_1 indicates the component already present in the uncorrelated wave function, $^3D_1^T$ the component due to tensor correlations. The dotted lines give the separate contribution of the one-body current, the dot-dashed lines the sum of the one-body and seagull currents, the dashed lines the sum of the one-body, seagull and pion-in-flight currents and the solid lines the total result, where also the contribution of the Δ -current is added.

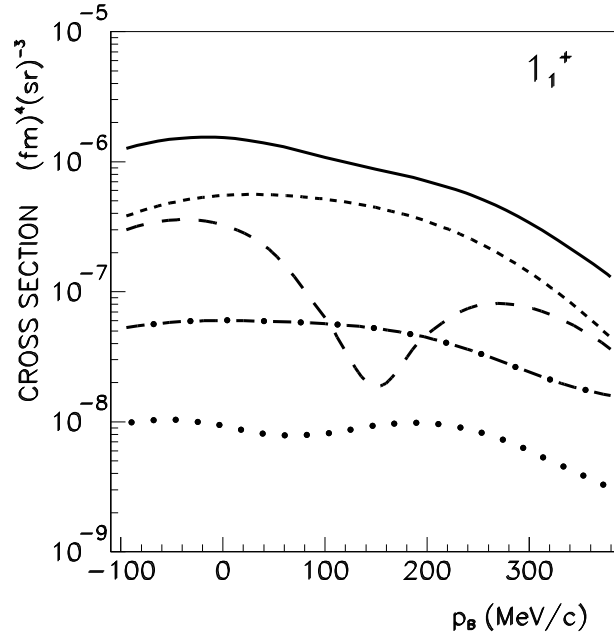


FIG. 5. The same as Fig. 2 but with the simpler approach of Ref. [10] for the two-nucleon overlap. The single-particle wave functions are taken from Ref. [27] and the correlation function from Ref. [28]. Line convention as in Fig. 2.

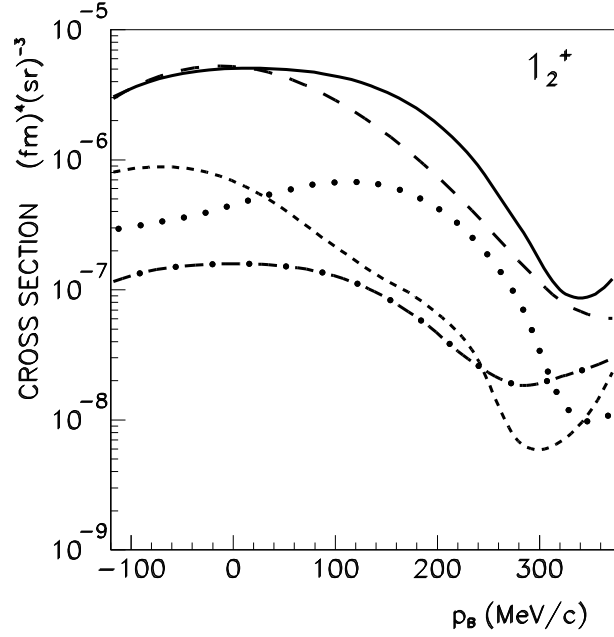


FIG. 6. The same as Fig. 2 for the transition to the 1_2^+ state of ^{14}N ($E_{2m} = 26.91$ MeV).

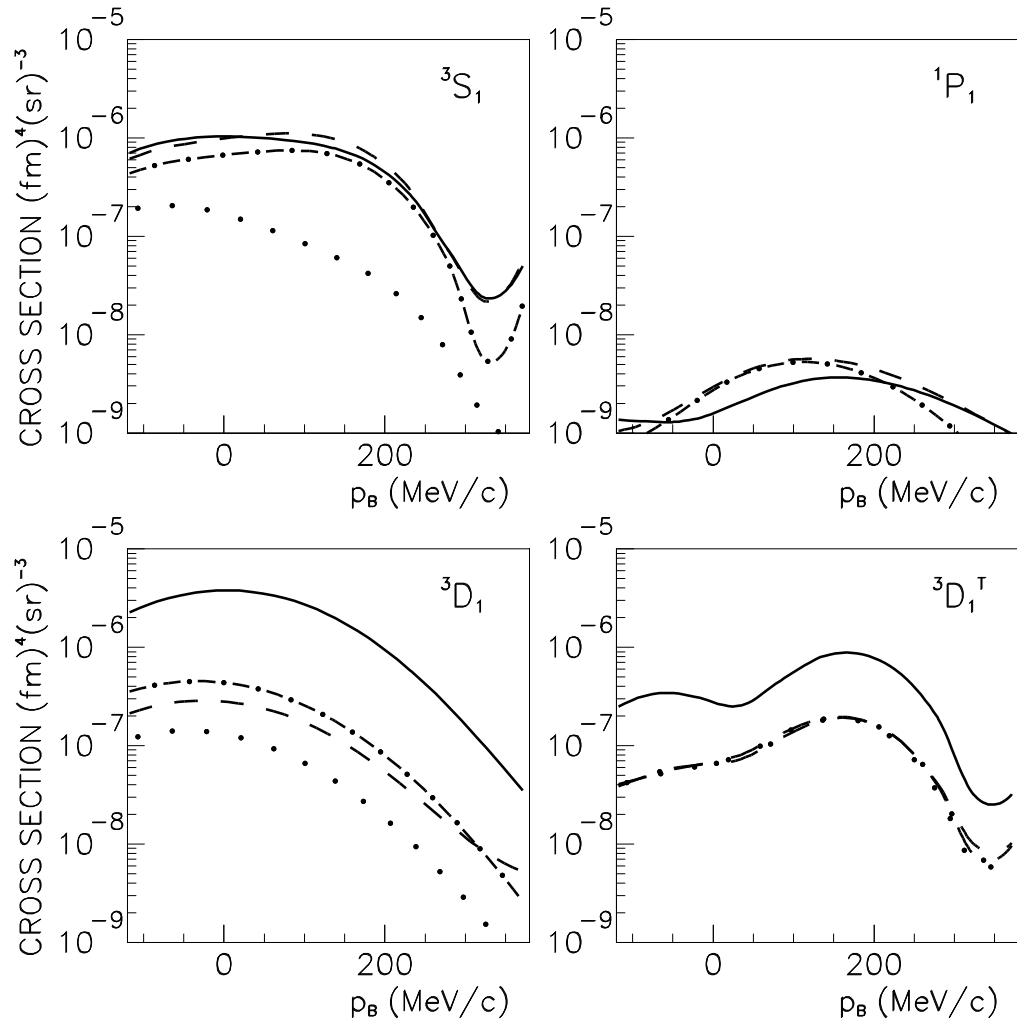


FIG. 7. The same as Fig. 4 for the transition to the 1_2^+ state of ^{14}N .

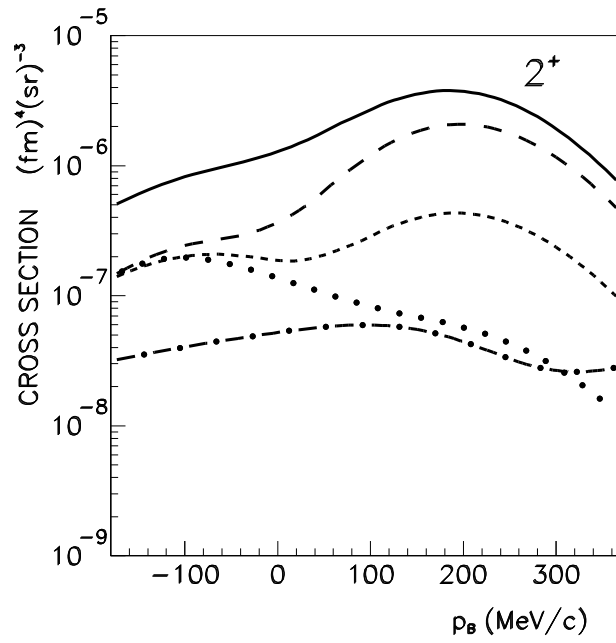


FIG. 8. The same as Fig. 2 for the transition to the 2^+ state of ^{14}N ($E_{2m} = 29.99 \text{ MeV}$).

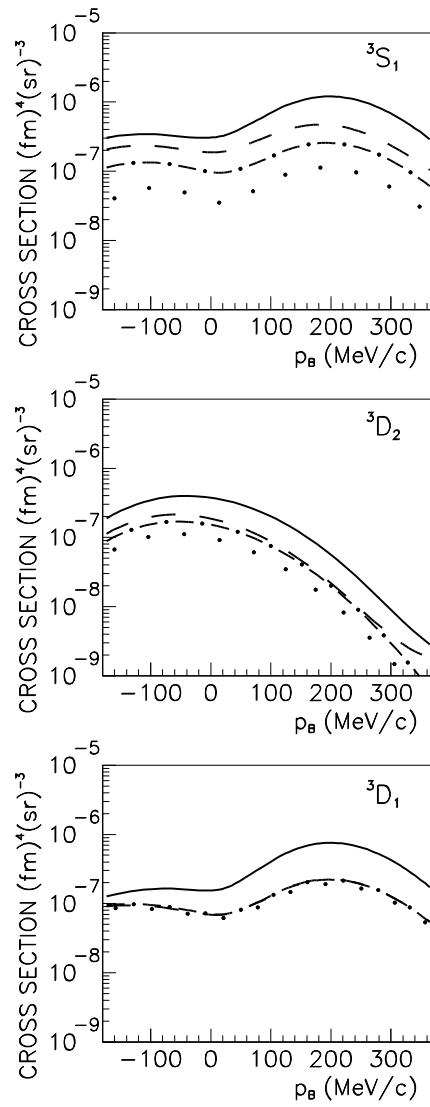


FIG. 9. The differential cross section of the $^{16}\text{O}(e,e'pn)$ reaction as a function of the recoil momentum p_B for the same transition and in the same kinematics as in Fig. 8. The optical potential is taken from Ref. [26]. Separate contributions of different partial waves of relative motions are drawn: 3S_1 , 3D_2 , 3D_1 . Line convention as in Fig. 4